International Journal of Thermal Sciences 139 (2019) 129–143

Contents lists available at ScienceDirect

International Journal of Thermal Sciences

journal homepage: www.elsevier.com/locate/ijts

An analytical approach based on Green's function to thermal response factors for composite planar structure with experimental validation

Milica Mirković Marjanović[a], Radovan Gospavić[b,*], Goran Todorović[b]

[a] Institute for Testing of Materials-IMS, Bulevar Vojvode Mišića 43 St., 1100, Belgrade, Serbia
[b] Faculty of Civil Engineering, University of Belgrade, Bulevar Kralja Aleksandra 73, 1100, Belgrade, Serbia

ARTICLE INFO

Keywords:
Green's functions
Heat conduction
Composite structure
Thermal response factors

ABSTRACT

The unsteady heat conduction in composite planar structure, with arbitrary number of layers, using analytical approach based on Green's Functions (GF) is analyzed. The analytical solution for spatial and temporal temperature distribution is evaluated in the general form and expressed in the terms of the convolution integrals. The GF are employed in the novel approach for calculation of Thermal Response Factors (TRF) with arbitrary shape functions for unsteady heat conduction in composite planar structure. The two pairs of TRF for spatial and temporal distribution of the temperature and the thermal flux are obtained. The whole analysis is performed in the time domain. A numerical scheme for efficient evaluation of convolution integral suitable for practical application in the case of the long term measurements with lower sampling rates is developed. The in-situ measurements of inside and outside surface temperatures and outside heat flux for a building wall under real dynamical environmental conditions during the period of then days are used for validation of the presented results and to demonstrate the possible practical application. Using developed approach and recorded surface temperatures as inputs the temporal and spatial distributions of the temperature and the thermal flux are obtained. These results are compared with experimental data and numerical simulations obtained by the Finite Volume Method (FVM).

1. Introduction

The composite planar structures have wide range of possible applications in engineering and technology. The structural and thermal properties of multilayer building components play a vital role not only in hygrothermal and acoustic comfort but also in energy performance of building's envelope. Accordingly, the heat transfer in composite structures under dynamical conditions is of the great importance in building energy efficiency [1–6]. The heat conduction and diffusion-type problems in multi-layer structures, coating/substrate system and functionally graded materials have been widely investigated theoretically and experimentally in a wide range of application areas such are industrial, bio-medical, electrical and building design [7–10].

The frequency response functions have been employed by Haibo Zhang et al. to obtain the three dimensional steady state temperature distributions in half-space multi-layer coatings subjected to heat flux at top surface [7]. The solution has been obtained in frequency domain corresponding to spatial coordinates. The steady-state spatial temperature distribution is expressed using temperature influence coefficients [7,11]. The 2D-filter solution has been utilized in inverse heat conduction problem for heat flux estimation during cryogen spray cooling by Jia-meng et al. [8]. The analytical solution in the frequency domain for unsteady heat transfer in multilayer building system, which is used for non-destructive testing purposes based on infrared thermography, has been proposed by C. Serra et al. [9].

The approach based on GF has been extensively used for the heat transfer and diffusion-type problems by many authors as it compactly describes the solution of the considered problem in integral representation [12–16].

The GF approach has been applied for vertical ground heat exchanger in anisotropic multilayer medium taking into account thermal conduction, advection and dispersion mechanisms [12]. On similar manner GF in analytical form has been utilized for nonlinear transient heat transfer problem in functionally graded hollow cylinder [13]. The simulation based on exact GF for unsteady reaction dynamics have been developed by Z. Bashardanesh and P. Lötstedt [16].

The Fourier and Laplace transformations are also important approaches which have been utilized to obtain analytical solutions of time-dependent heat conduction problems in frequency domain [17–21]. Among the studies on composite structures, N. Simões et al.

* Corresponding author.
E-mail address: gospavic@grf.bg.ac.rs (R. Gospavić).

https://doi.org/10.1016/j.ijthermalsci.2019.01.020
Received 28 May 2018; Received in revised form 11 December 2018; Accepted 16 January 2019
1290-0729/

[17] developed semi-analytical solution for temperature distribution based on GF in frequency domain for multilayer 3D structure unbounded in lateral directions using time and spatial Fourier transform. The system has been subjected to heat source placed inside material.

The possible difficulty related to semi-analytical analysis in the frequency domain is that matching conditions between layers must be imposed at all considered frequencies, which can slowdown simulation and inevitably increase the CPU and memory requirements. In the general case, for multilayer structures, the analytical solution in the frequency domain become formidable and precludes obtaining the analytical solution in the time domain [21]. X. Luo et al. [22] used a thermal resistance network method to analyze the heat transfer in electronic packaging with upper and lower surfaces cooling. The analytical solution has been obtained and utilized for calculation of the thermal resistance and temperature prediction.

The transient heat conduction subject to uncertain random heat conductivity and capacity has been analyzed using stochastic approach by D. Xiu and G. E. Karniadakis [23]. The generalized polynomial chaos algorithm has been implemented. This approach was based on spectral expansion of random variables by the orthogonal polynomials from the Askey scheme.

D. Xiu and J.S. Hesthaven [24] developed high-order stochastic collocation approach for solving partial differential equations with random inputs as valuable alternative to traditional Monte Carlo methods and stochastic Galerkin methods.

The analytical solutions in the time domain for unsteady heat conduction and diffusion-type problems in composite structures under mixed type of Boundary Conditions (BC) have been studied systematically by Ozisk [25] and G. P. Mulholland [26]. In this approach the original problem with inhomogeneous mixed BC is transformed using some kind of axillary functions to equivalent problem with homogeneous BC. The transformed problem is solved using the method of separation of variables and Duhamel's principle [25–27]. The main advantage of this approach is that GF depends only on physical properties and dimensions of considered composite structure and corresponding eigenvalue problem which incorporates matching conditions on layer interfaces has to be solved only once.

The TRF and Conduction Transfer Functions (CTF) have been widely utilized in simulations of conduction heat transfer in the planar composite structures [10,28–31]. The TRF method is based on superposition principle and linear nature of the heat equation. In standard approach TRF are defined as responses to excitation by unit triangle pulse at different sampling time instants. The Laplace transform, state space method and analysis in the frequency domain are the most widely used approaches for calculation of CTF and TRF. The main disadvantage related to the Laplace method is calculation of the poles in complex domain which can increase computational time and results in numerical errors. The state space method is based on matrix algebra to obtain TRF and it avoids searching poles but it can be computational costly when the number of spatial nodes are increased [29].

To reduce the number of terms in TRF convolution series and speed up calculations, the CTF approach has been proposed [28,29]. The second order shaping functions for calculation of TRF has been used by Jose Manuel et al. [10]. The modified CTF method with higher order discretization scheme has been applied for prediction of surface heat flux from the building wall surface temperatures as inputs by C. Luo et al. [30]. These predictions are compared with original CTF, FVM and heat transfer matrix method. The three different methods for calculation of CTF coefficients, namely direct root-finding, state-space and frequency-domain regression have been investigated by Xiang Qian Li et al. [31].

In this study the novel approach based on GF for calculation of TRF for composite planar structures is proposed. The detailed evaluation of TRF from analytical GF is presented, based on the analytical method developed by Ozisk [25] and G. P. Mulholland [26] for multilayer planar structure. The influence of the interface thermal resistance (ITR) on the spatial and temporal temperature and heat flux distribution has been analyzed as well.

Presented approach for TRF calculation has advantages over standard methods based on the Laplace transform (direct-root finding) and the Fourier expansion. Unlike the Laplace's method the whole analysis is performed in the time domain and in that way it avoids searching poles in the complex plane. Nevertheless, the GF depends only on the physical properties and thickness of composite layers and can be reused in TRF calculation for different spatial positions reducing the computational time. The similar advantage applies in comparison with numerical methods such is FVM, as the same GF functions can be reused in calculations for different inside and outside surface temperature profiles. On the other side the FVM simulation must be repeated for each new temperature profiles. Another possible advantage of TRF over FVM is related to calculation for the very long time intervals as the computational times in the case of TRF approach are considerably shorter.

As the recorded temperatures are obtained only at discrete time points the convolution integral for the real in-situ measurements is evaluated numerically. On the other hand, the GF used in analytical solution exhibit very rapid exponential rate of change which is much higher than usual rate of change in recorded data. Using the same size of the time step in numerical evaluation of convolution integrals as one in the recorded data may lead to high inaccuracy in prediction results especially for lower sampling rates and long term measurements. The simple resampling of the input data set would reduce this problem but this will slow down the whole simulation. The numerical evaluation of convolution integrals has been modified to adjust the rate of changes in GF and recorded data. This numerical scheme aims to increase accuracy of predicted results and considerably speed up calculations. On this way the accurate and efficient analytical approach for analysis of non-stationary conductive heat transfer in the planar composite structure with different types of BC which is suitable for practical applications and calculation of the TRF is developed. The proposed method has been used to obtain the two pairs of TRF for spatial and temporal distribution of the temperature and the thermal flux.

Another objective was validation of the developed analytical approach and to demonstrate possible practical application. To aim this objective in-situ measurements of inside and outside surface temperatures and outside surface heat flux, obtained under real environmental conditions, for the building wall have been utilized. The recorded surface temperatures have been used as input data set in the TRF calculations and FVM simulation for prediction of the outside thermal flux and heat losses. These predictions are compared with experimental data; also temporal distributions of the internal surface heat flux obtained by the presented approach are compared with numerical results evaluated by the FVM. The influence of ITR on the temporal and spatial temperature and heat flax distribution has been analyzed as well. All numerical calculations are performed in computer software developed in the programing language Python.

2. Experimental set up

The in-situ measurements of inside and outside surface temperatures and outside surface thermal flux have been performed in period from 2nd to 17th March of 2017 on an external building wall of one flat in a four-storey residential building located in Belgrade, Serbia. The flat was located on the fourth floor, while the façade wall was oriented towards the north, sheltered from direct sun light. On this way the direct impact of solar radiation is excluded. As only surface quantities are recorded, only conductive processes inside the building structure are taken into account without influence of the boundary layer. The considered composite building structure was consisted of 5 homogeneous layers, with dimensions and thermal properties presented in Table 1. The complete measurements have been organized as standalone experimental set up. The instrumentation has been consisted of two temperature sensors (TSs) and one heat flux meter (HFM). The TSs

Table 1
Dimensions and thermal properties of the wall composites.

layer No.	Layer	Thickness ℓ [m]	Density ρ [kg/m^3]	Specific heat c [$J/kg{\cdot}K$]	Thermal conductivity λ [$W/m{\cdot}K$]
1	Interior plaster (inside layer)	0.02	800	1090	0.7
2	Solid brick	0.25	1800	920	0.76
3	Mortar	0.01	1900	1050	0.99
4	Mineral rock wool	0.12	23	840	0.034
5	Exterior façade plaster (outside layer)	0.02	1900	1050	0.7

are based on NiCr−Ni type thermocouples with following characteristics: a wire diameter: 1.5 mm, measurement range from $-200^{\circ}C$ to $+1200^{\circ}C$, response time to step excitation in air: 15 s and sensitivity: 41 μV/°C. The TSs have been connected to a digital thermometer with built-in digital data logger with 12-*bit* A/D convertor, also the logger has reference junction temperature of $0^{\circ}C$ automatically adjusted. The temperature was measured with an uncertainty of ± 0.2°C, within the range of [-100°C, +100°C].

HFM was silicone greenTeg flux meter with following characteristics: ultra-high resolution anodized aluminum surface material, sensing dimensions: 30 mm × 30 mm *x* 2.2 mm; operating temperature range min/max: −50/150°C; and minimum sensitivity: 7 μV/(W/m^2) [32]. HFM was connected with the data loggers with the resolution of 12 *bits* and measuring frequency: 50/*s* to 2/*day*. The TSs were placed on the inside and outside surface of the wall, at the same position relative to the edges of the wall. The HFM was placed on the top of the outside TSs to measure outside surface heat flux at the same location as surface temperature did. To achieve good thermal contact between the HFM and the wall surface the thermal compound paste, with the thermal conductivity of 5 W/mK, was used. The influence of the HFM on the temperature distribution can be neglected due to its small dimensions. The all collected data are recorded automatically in the all course of experiment. The temperature data from TSs and digital data logger was collected online through RS323 port on PC computer. The inside and outside surface temperature data are automatically read every second and the mean value for every 5 min are calculated and recorded. A computer program for automatic reading, acquisition and saving of collected data has been developed in the programing language C. All data are recorded simultaneously with sampling frequency of 1/(5min). A photographic view of the experimental setup and instrumentation is presented in Fig. 1.

3. Mathematical model

The non-stationary conductive heat transfer in the N-layer composite planar structure is modeled by the following heat equation, with corresponding initial, boundary and matching conditions [33,34]:

$$\frac{\partial T_n(x,\,t)}{\partial t} = \frac{1}{\rho_n{\cdot}c_n}{\cdot}\frac{\partial}{\partial x}\left(\lambda_n{\cdot}\frac{\partial T_n(x,\,t)}{\partial x}\right);\quad x\in[x_{n-1},\,x_n];\quad n=1,\,\cdots,N;$$

$$T_n(x,\,t=0)=T_0(x),\quad x\in[x_{n-1},\,x_n];\ n=1,\,\cdots,N;$$

$$T_1(x=0,\,t)=T_{in}(t),\quad T_N(x=0,\,t)=T_{out}(t),$$

$$(T_{n+1}(x,\,t)-T_n(x,\,t))|_{x=x_n} = r_n{\cdot}\lambda_n\frac{\partial T_n(x,\,t)}{\partial x}\bigg|_{x=x_n};\ \lambda_n\frac{\partial T_n(x,\,t)}{\partial x}\bigg|_{x=x_n} = \lambda_{n+1}\frac{\partial T_{n+1}(x,\,t)}{\partial x}\bigg|_{x=x_n};\ n=1,\,\cdots,N-1;$$

$$x_0=0,\ x_1=\ell_1,\ x_2=\ell_1+\ell_2,\ \cdots,x_N=\ell_1+\ell_2+\cdots+\ell_N=L,\ t\geq 0,$$

where the wall consists of N planar layers arranged along x-axes, the layers are labeled with index n, while λ_n , ρ_n, c_n and ℓ_n are thermal conductivity, density, specific heat and thickness of nth layer, respectively. The all thermal characteristics are considered to be constant inside the each layer. The quantity $T_n(x,\,t)$ is the temperature distribution in the nth layer, $T_0(x)$ is the initial temperature distribution inside the wall at time instant $t=0$. The quantities $T_{in}(t)$ and $T_{out}(t)$ are temporal variations of inside ($x=0$) and outside ($x=L$) surface temperatures respectively, x_n are x-coordinates of layer contacts and r_n are the ITRs between nth and $(n+1)^{th}$ layers respectively. The ITRs at nth interface is modeled as equivalent air gap between nth and $(n+1)^t$ layers as:

$r_n=\delta_n/\lambda_{air}$ where λ_{air} is air thermal conductivity and δ_n is equivalent thickness of the air gap between layers. The whole structure has thickness equal to L and the coordinate origin is at the beginning of the first layer. The direction of x-axes is adopted as the reference direction for all thermal fluxes. The first three relations in Eq. (2) represent the initial, boundary and matching conditions, respectively. The problem presented by Eqs.(1) and (2) belongs to the class of Boundary Value Problems (BVP). It should be noted, that the Dirichlet BC are prescribed only on the external boundaries ($x=0$ and $x=L$), while the Robin type matching conditions are prescribed on the interfaces. The geometry of the considered structure is shown in Fig. 2.

The above problem can be solved analytically by using of the following transformation [25,26]:

$$T_n(x,\,t)=T_n^*(x,\,t)+U(x,\,t),\quad U(x,\,t)=T_{in}(t){\cdot}f_1(x)+T_{out}(t){\cdot}f_2(x),\tag{3}$$

where $T_n^*(x,\,t)$ is transformed temperature on nth segment and $f_{1,2}(x)$, $U(x,\,t)$ are axillary functions. The $f_{1,2}(x)$ are functions which satisfy the next conditions:

$$f_1(x=0)=1,\quad f_1(x=L)=0,\quad f_2(x=0)=0,\ f_2(x=L)=1,$$

$$f_{1,2}(x)|_{x=x_n+\varepsilon}-f_{1,2}(x)|_{x=x_n-\varepsilon}=r_n{\cdot}\lambda_n{\cdot}\frac{\partial f_{1,2}(x)}{\partial x}\bigg|_{x=x_n-\varepsilon}$$

$$\lambda_n{\cdot}\frac{\partial f_{1,2}(x)}{\partial x}\bigg|_{x=x_n-\varepsilon}=\lambda_{n+1}{\cdot}\frac{\partial f_{1,2}(x)}{\partial x}\bigg|_{x=x_n+\varepsilon},\ \varepsilon\to 0;\quad n=1,\,\cdots,N-1;$$

where ε is infinitesimal small quantity. Using transformation from Eqs. (3) and (4), the governing Partial Differential Equation (PDE) with corresponding boundary and initial conditions given by Eqs. (1) and (2), is transformed as follows:

$$\frac{\partial T_n^*(x,\,t)}{\partial t}-\frac{1}{\rho_n{\cdot}c_n}{\cdot}\frac{\partial}{\partial x}\left(\lambda_n{\cdot}\frac{\partial T_n^*(x,\,t)}{\partial x}\right)=F(x,\,t);\ x\in[x_{n-1}x_n];\ n=1,\,\cdots,N:$$

$$T_1^*(x=0,\,t)=0,\ T_N^*(x=L,\,t)=0;$$

$$T_n^*(x,\,t=0)=T_0(x)-U(x,\,0)=T_0^*(x),\quad F(x,\,t)=\frac{\partial U(x,\,t)}{\partial t}-\frac{1}{\rho_n{\cdot}c_n}{\cdot}\frac{\partial}{\partial x}\left(\lambda_n{\cdot}\frac{\partial U(x,\,t)}{\partial x}\right),$$

where $T_0^*(x)$ is the initial condition for the transformed temperature $T_n^*(x,\,t)$ at time $t=0$ and function $F(x,\,t)$ is defined on the whole domain $x\in[O,\,L]$. On this way the initial BVP with non-homogeneous BC is transformed to BVP with homogeneous BC with additional non-homogeneous term $F(x,\,t)$ in the governing PDE. It should be noticed

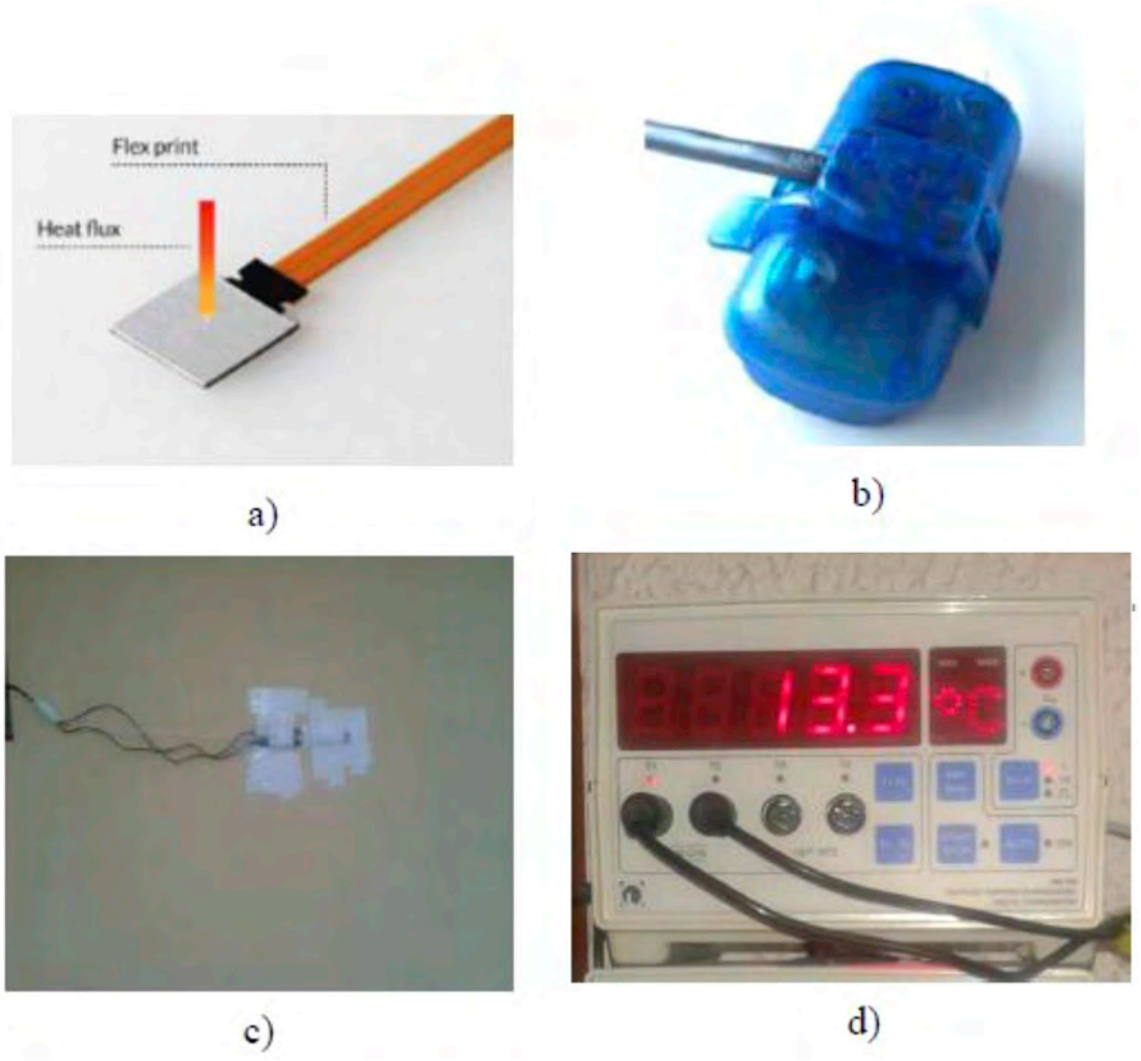

Fig. 1. A photographic view of experimental setup and instrumentation a) Silicon "g-Skin" flux meter sensor. b) Flux meter data logger with surface connector c) The measurement site on the outside façade wall d) digital data logger for TSs.

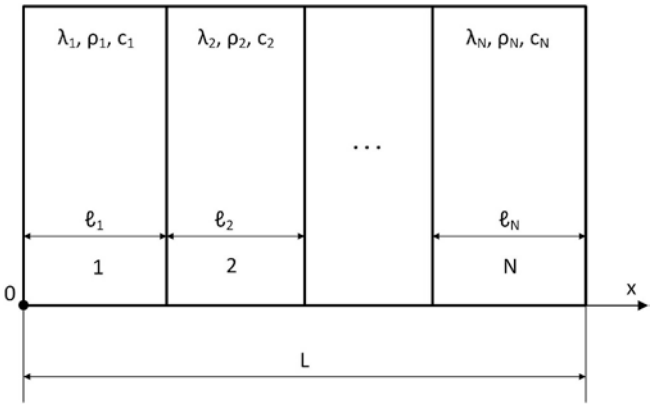

Fig. 2. The geometry of the considered N-layer problem.

that even the spatial derivative of the all relevant functions in Eqs. 1-5, ($f_{1,2}$, F and U) has discontinuous first derivative on the interfaces, the term which correspond to the second derivative.

$\frac{\partial}{\partial x}\left(\lambda_n \cdot \frac{\partial U(x,t)}{\partial x}\right)$ in Eq. (5) will always be finite because the term $\lambda_n \cdot \partial U/\partial x$ is continues and does not contain any jumps on the interfaces. On this way it is possible to get physically meaningful solution of Eq. (5) on any segment $\in [x_{n-1}, x_n]$.

One particular solution of the associated homogeneous problem in Eq. (5) can be obtained by the method of separation of variables such as $exp(-\beta^2 \cdot t) \cdot \varphi_n(x)$, where β is separation constant and $\varphi_n(x)$ is solution of the following regular Strum-Liouville problem [25,26]:

$$\frac{\partial}{\partial x}\left(\lambda_n \cdot \frac{\partial \varphi_n(x)}{\partial x}\right) + \beta^2 \cdot \rho_n \cdot c_n \cdot \varphi_n(x) = 0, \quad x \in [x_{n-1}, x_n]; \quad n = 1, \cdots, N;$$

$$\varphi_{n=1}(0) = \varphi_{n=N}(L) = 0,$$

$$(\varphi_{n+1}(x) - \varphi_n(x))|_{x=x_n} = r_n \cdot \lambda_n \frac{\partial \varphi_n(x)}{\partial x}\bigg|_{x=x_n}; \ \lambda_n \frac{\partial \varphi_n(x)}{\partial x}\bigg|_{x=x_n} = \lambda_{n+1} \frac{\partial \varphi_{n+1}(x)}{\partial x}\bigg|_{x=x_n}; n = 1, \cdots, N-1.$$

The solution of the above problem at segment $x \in [x_{n-1}, x_n]$ is:

$$\varphi_n(x) = A_n \cdot \sin\left(\frac{\beta}{\sqrt{k_n}} \cdot x\right) + B_n \cdot \cos\left(\frac{\beta}{\sqrt{k_n}} \cdot x\right); \ n = 1, \cdots, N; \tag{7}$$

where $k_n = \lambda_n/\rho_n \cdot c_n$.

From the BC at $x = 0, L$ in Eq. (6) follows that $B_1 = 0$ and $B_N = -A_N \tan(L \cdot \beta/\sqrt{k_N})$ respectively. Using matching conditions from Eq. (6) and Eq. (7) the next homogeneous system of $2 \times (N-1)$ linear

$$\begin{bmatrix} & b_1\cdot\cos(\theta_{11}) + \sin(\theta_{11}) & & 0 & \cdots & 0 \\ & -\sin(\theta_{11}) - \cos(\theta_{11}) & & & & \\ a_1\cdot\cos(\theta_{11}) & - a_2\cdot\cos(\theta_{12}) & a_2\cdot\sin(\theta_{12}) & 0 & \cdots & 0 \\ 0 & b_2\cdot\cos(\theta_{22}) + \sin(\theta_{22}) & - b_2\cdot\sin(\theta_{22}) + \cos(\theta_{22}) & - \sin(\theta_{23}) & - \cos(\theta_{23}) & 0\cdots 0 \\ 0 & a_2\cdot\cos(\theta_{22}) & - a_2\cdot\sin(\theta_{22}) & - a_3\cdot\sin(\theta_{23}) & a_3\cdot\sin(\theta_{23}) & 0\cdots 0 \\ \cdots & \cdots & \cdots & \cdots & \cdots & \cdots \\ 0 & \cdots & 0 & b_{N-1}\cdot\cos(\theta_{N-1,N-1}) & - b_{N-1}\cdot\sin(\psi_{N-1,N}) & - (\sin(\theta_{N-1,N}) \\ & & & + \sin(\theta_{N-1,N-1}) & + \cos(\theta_{N-1,N}) & - \cos(\theta_{N-1,N})\cdot\mathrm{tg}(\theta_{N,N})) \\ 0 & \cdots & 0 & a_{N-1}\cdot\cos(\theta_{N-1,N-1}) & - a_{N-1}\cdot\sin(\theta_{N-1,N-1}) & - a_{N-1}\cdot(\cos(\theta_{N-1,N}) \\ & & & & & + \sin(\theta_{N-1,N})\cdot\mathrm{tg}(\theta_{N,N})) \end{bmatrix}$$

$$\cdot\begin{bmatrix} A_1 \\ A_2 \\ B_2 \\ A_3 \\ B_3 \\ \vdots \\ A_{N-1} \\ B_{N-1} \\ A_N \end{bmatrix} = \begin{bmatrix} 0 \\ \vdots \\ 0 \end{bmatrix} \tag{8}$$

equations is assembled:
where $\theta_{ij} = x_i\cdot\beta/\sqrt{k_j}$, $a_i = \beta\cdot\lambda_i/\sqrt{k_i}$ and $b_i = r_i\cdot a_i$.

To have a non-trivial solution of the above system the determinant of the system must be equal to zero. This condition leads to a transcendental equation whose roots are eigenvalues β_i. The number of eigenvalues are infinite and in the further analysis they are labeled with index i and ordered as $\beta_1 < \beta_2 < \beta_3 < \cdots$. The eigenfunctions $\varphi_i(x)$ which correspond to eigenvalue β_i are defined on the whole domain $x \in [0, L]$ using Eq. (7) on the following way:

$$\varphi_i(x) = A_{n,i}\cdot\sin\left(\frac{\beta_i}{\sqrt{k_n}}\cdot x\right) + B_{n,i}\cdot\cos\left(\frac{\beta_i}{\sqrt{k_n}}\cdot x\right), \quad x \in [x_{n-1}, x_n] \quad ; \quad n = 1, \cdots, N; \tag{9a}$$

where quantities $A_{n,i}$ and $B_{n,i}$ correspond to eigenvalue β_i and they are labeled with additional index i.

As the differential operator in Eq. (6) is self-adjoint, all eigenfunctions are orthonormal and β_i are real [35]. To form orthonormal set of eigenfunctions, the following conditions must be imposed:

$$\sum_{n=1}^{N}\int_{x_{n-1}}^{x_n}\varphi_i(x)\cdot\rho_n\cdot c_n\cdot\varphi_j(x)\cdot dx = \delta_{ij}, \qquad \delta_{ij} = \begin{cases} 1, & i = j \\ 0, & i \neq j \end{cases}, \tag{9b}$$

where δ_{ij} is Kronecker delta symbol. Once when eigenvalues β_i are obtained the unknown quantities $A_{n,i}$ and $B_{n,i}$ can be determined from Eqs. (6), (8) and (9b) for each β_i.

Using Duhamel's principle, the solution of the problem defined in Eq. (5) can be expressed in the whole domain by the next relation [25,36,37]:

$$T^*(x, t) = \int_0^L H(x, y, t)\cdot T_0^*(y)\cdot dy + \int_0^t\int_0^L H(x, y, t-s)\cdot F(y, s)\cdot dy\cdot ds, \quad x \in [0, L]. \tag{10}$$

The first term in the above equation is a particular solution of the problem in Eq. (5) due to the initial conditions $T_0^*(x)$. The function $H(x, y, t)$ is Green's function or fundamental solution of the associated homogeneous problem in Eq. (5) and can be expressed in the following form [25]:

$$H(x, y, t) = \sum_{i=1}^{+\infty}\exp(-\beta_i^2\cdot t)\cdot\varphi_i(x)\cdot c_n\cdot\rho_n\cdot\varphi_i(y), \quad y \in [x_{n-1}, x_n] \quad ; \quad n = 1, \cdots, N; \tag{11}$$

where x_n are coordinates of the contacts between nth and $(n+1)^{th}$ layers defined in Eq. (2) and spatial coordinates y is inside nth layer. The second term in the first relation in Eq. (10) can be evaluated such as:

$$\int_0^t\int_0^L H(x, y, t-s)\cdot F(y, s)\cdot dy\cdot ds = \sum_{i=1}^{+\infty}\left(\varphi_i(x)\cdot\exp(-\beta_i^2\cdot t)\cdot\int_0^t F,\ \varphi_i\cdot\exp(\beta_i^2\cdot s)\cdot ds\right),$$

$$F,\ \varphi_i = \sum_{n=1}^{N}\int_{x_{n-1}}^{x_n} F(y, s)\cdot\rho_n\cdot c_n\cdot\varphi_i(y)\cdot dy,$$

where integration in spatial coordinate y over domain $[0, L]$ is replaced by sum of integrals over each layer and.

$F,\ \varphi_i$ are coefficients in Orthogonal Series Expansion (OSE) of function F.

The above relations can be further transformed using Eqs.(5) and (6) and partial integrations as follows:

$$\begin{aligned}\int_0^t F,\ \varphi_i\cdot\exp(\beta_i^2\cdot s)\cdot ds = &-\int_0^t\sum_{n=1}^{N}\exp(\beta_i^2\cdot s)\cdot\left[\int_{x_{n-1}}^{x_n}\left(\rho_n\cdot c_n\cdot\frac{\partial U(x, s)}{\partial t} - \lambda_n\frac{\partial^2 U(x, s)}{\partial x^2}\right)\cdot\varphi_i(x)\cdot dx\right]\\ &\cdot ds = -\exp(\beta_i^2\cdot t)\cdot U(x, t),\ \varphi_i + U(x, t_0),\ \varphi_i\\ &+\int_0^t\exp(\beta_i^2\cdot s)\cdot\left(\lambda\cdot\frac{\partial U(x, s)}{\partial x}\cdot\varphi_i(x) - \lambda\cdot U(x, s)\cdot\frac{\partial\varphi_i(x)}{\partial x}\right)\Big|_0^L\cdot ds,\end{aligned} \tag{13}$$

where: $U(x, t),\ \varphi_i = \sum_{n=1}^{N}\int_{x_{n-1}}^{x_n}\rho_n\cdot c_n\cdot U(x, t)\cdot\varphi_i(x)\cdot dx$ are expansion coefficients of function $U(x, t)$, $\lambda(0) = \lambda_1$ and $\lambda(L) = \lambda_N$. Finally,

substituting Eq. (13) back to Eq. (12) and taking into account Eqs. (3) and (4) the temperature distribution in the whole domain at time instant $t > 0$ can be expressed by the next relation:

$$T(x,\,t) = T_{ic}(x,\,t) + \delta U(x,\,t) + \sum_{i=1}^{+\infty} \varphi_i(x) \cdot \int_0^t exp(-\beta_i^2 \cdot (t-s)) \cdot \left(\lambda \cdot \frac{\partial U(x,\,s)}{\partial x} \cdot \varphi_i(x) - \lambda \cdot U(x,\,s) \cdot \frac{\partial \varphi_i(x)}{\partial x} \right) \Big|_0^L \cdot ds\,,$$

$$\delta U(x,\,t) = U(x,\,t) - \sum_{i=1}^{+\infty} \varphi_i(x) \cdot U(x,\,t),\, \varphi_i\,, \quad T_{ic} = \sum_{i=1}^{+\infty} exp(-\beta_i^2 \cdot t) \cdot \varphi_i(x) \cdot T_0,\, \varphi_i\,, \quad x \in [0,\,L],$$

$$T_0,\, \varphi_i = \sum_{n=1}^{N} \int_{x_{n-1}}^{x_n} \rho_n \cdot c_n \cdot T_0(x) \cdot \varphi_i(x) \cdot dx\,,$$

where $T_{ic}(x,\,t)$ is particular solution of the original problem from Eq. (1) due to initial conditions $T_0(x)$ prescribed at the time instant $t = 0$ and $T_0,\, \varphi_i$ are coefficients in OSE for function $T_0(x)$. The above equation is given in the general form. Taking into account Eqs. (3), (4) and (6) the relation for temperature distribution with Dirichlet BC reads:

$$T(x,\,t) = T_{ic}(x,\,t) + \Delta_1 \cdot T_{in}(t) + \Delta_2 \cdot T_{out}(t) + \sum_{i=1}^{M} \varphi_i(x) \cdot \int_0^t exp(-\beta_i^2 \cdot (t-s)) \cdot \left(\lambda_1 \cdot T_{in}(s) \cdot \frac{\partial \varphi_i(x)}{\partial x}\Big|_{x=0} - \lambda_N \cdot T_{out}(s) \cdot \frac{\partial \varphi_i(x)}{\partial x}\Big|_{x=L} \right) \cdot ds$$

$$\Delta_{1,2}(x) = f_{1,2}(x) - \tilde{f}_{1,2};\;\; \tilde{f}_{1,2} = \sum_{i=1}^{M} \varphi_i(x) \cdot f_{1,2},\, \varphi_i;\;\; f_{1,2},\, \varphi_i = \sum_{n=1}^{N} \int_{x_{n-1}}^{x_n} \rho_n \cdot c_n \cdot f_{1,2} \cdot \varphi_i(x) \cdot dx\,,$$

where $\tilde{f}_{1,2}(x)$ are truncated OSEs of the functions $f_{1,2}(x)$ with M terms. Now, the experimental data $T_{in}(t)$ and $T_{out}(t)$ appears explicitly in Eq. (15). In considerations from Eq. (1) to Eq. (11) we mainly follow the procedure similar to Ozisk [25] and G. P. Mulholland [26] except that the Dirichlet BC has been imposed and the weaker set of conditions for axillary functions $f_{1,2}(x)$ defined by Eq. (4) have been applied, namely Ozisk [25] and G. P. Mulholland [26] imposed following additional conditions:

$$\frac{\partial^2 f_{1,2}(x)}{\partial x^2} = 0 \Rightarrow \frac{\partial^2 U(x,\,t)}{\partial x^2} \equiv 0. \tag{16}$$

Under conditions in Eq. (16) the functions $f_{1,2}(x)$ can be expressed in analytical form as piecewise linear steady state temperature distributions in the considered composite structure for the following surface temperatures:

$T_{in} = 1$, $T_{out} = 0$ for $f_1(x)$ and $T_{in} = 0$, $T_{out} = 1$ for $f_2(x)$ [25,26]. Even there is no any specific physical reason to prescribe constraint in Eq. (16), these additional conditions considerably simplify the solution and analysis of the problem but they cannot be imposed under Neuman BC or any combination with this type of BC. On the other hand the presented procedure from Eq. (12) to Eq. (15) is valid in the general case for different type of BC with modification of the first relation in Eq. (4). For an example under Neuman BC modified conditions in Eq. (4) are: $df_1/dx|_{x=0} = 1$, $df_1/dx|_{x=L} = 0$ and $df_2/dx|_{x=0} = 0$, $df_2/dx|_{x=L} = 1$.

The terms $\Delta_{1,2}$ in Eq. (15) presents difference between functions $f_{1,2}$ and its truncated OSE obtained by orthogonal set φ_i. As OSE converges uniformly for continuous functions, functions $\Delta_{1,2}(x)$ converge uniformly to zero in all points in domain $x \in (0,\,L)$ except at domain boundaries $x = 0,\, L$ where $\lim_{x\to 0} \Delta_1(x) = 1$ and $\lim_{x\to L} \Delta_2(x) = 1$. This is due to the fact that with Dirichel BC $\varphi_i(x = 0,\, L) = 0$, while functions $f_{1,2}$ take value one at the domain boundaries. According to this in the limit process, when $M \to +\infty$, functions $\Delta_{1,2}(x)$ in Eq. (15) have discontinuity at the domain boundaries. However the temperature distribution is continuous inside the whole domain which can be easily justified from Eq. (10) as all terms in this equations are continuous.

From this analysis follows that solution given by Eq. (15) do not depend on the arbitrary choice of the axillary functions $f_{1,2}(x)$ but only on $T_{in}(t)$ and $T_{out}(t)$ which is in accordance with uniqueness of solution of BVP.

As term T_{ic} in Eq. (15) is exponentially vanishing, according to Eq. (14), it can be neglected for all $t \gg t_0$ if the following condition is satisfied $\beta_1^2 \cdot t_0 \gg 1$, $t_0 > 0$. In this case the solution from Eq. (15) can be expressed in the form of convolution integrals such as:

$$T(x,\,t) = g_1 * T_{in} + g_2 * T_{out} = \int_0^t g_1(x,\,t-s) \cdot T_{in}(s) \cdot ds + \int_0^t g_2(x,\,t-s) \cdot T_{out}(s) \cdot ds, \quad t > t_0\,, \tag{17}$$

where the operator "* ", denotes the convolution operator and $g_{1,2}(x,\,t)$ are GF which represents the response on temperature excitations by Dirac delta functions on inside and outside surfaces respectively. The GF $g_{1,2}(x,\,t)$ with Dirichlet BC expressed in the analytical form are:

$$g_1(x,\,t) = \Delta_1(x) \cdot \delta(t) + \lambda_1 \sum_{i=1}^{\infty} \exp(-\beta_i^2 \cdot t) \cdot \varphi_i(x) \cdot \frac{\partial \varphi_i(x)}{\partial x}|_{x=0};$$
$$g_2(x,\,t) = \Delta_2(x) \cdot \delta(t) - \lambda_N \sum_{i=1}^{\infty} \exp(-\beta_i^2 \cdot t) \cdot \varphi_i(x) \cdot \frac{\partial \varphi_i(x)}{\partial x}|_{x=L}, \tag{18}$$

where $\delta(t)$ is Dirac delta function. Taking into account the limit values of functions $\Delta_{1,2}$ and BC for φ_i at the domain boundaries $x = 0,\, L$ the following relations hold: $g_1(x = 0,\, t) = g_2(x = L,\, t) = \delta(t)$ which is in accordance with Eq. (17). The heat flux at some spatial coordinate $x \in [x_{n-1},\, x_n]$ inside nth layer can be obtained using the following relation:

$$q(x,\,t) = -\lambda_n \cdot \frac{\partial T(x,\,t)}{\partial x} = -\lambda_n \cdot \left(\int_0^t \frac{\partial g_1(x,\,t-s)}{\partial x} \cdot T_{in}(s) \cdot ds + \int_0^t \frac{\partial g_2(x,\,t-s)}{\partial x} \cdot T_{out}(s) \cdot ds \right),$$

$$t > t_0, \quad x \in [x_{n-1},\, x_n]$$

The numerical procedure for efficient and accurate evaluation of the convolution integrals in Eqs (17,19) is presented in Appendix A. The presented approach has been extended on the cylindrical and spherical multilayer structures with distributed internal heat sources or sinks [25]. For the anisotropic type of the problem the two or three dimensional problem would have to be considered.

3.1. Evaluation of RTF using GF

The internal and external interpolated surface temperatures $\tilde{T}_{in,out}(t)$ can be expressed by the shape functions and the recorded surface temperatures $\tilde{T}_{in,out}(j \cdot \Delta t)$ at sampling times $j \cdot \Delta t$ by the following relation:

$$\tilde{T}_{in,out}(t) = \sum_{j=0}^{K} T_{in,out}(j \cdot \Delta t) \cdot \psi(t - j \cdot \Delta t), \quad \psi(t - j \cdot \Delta t) = \delta_{j0}, \quad 0 \le j \le M, \quad 0 \le t \le K \cdot \Delta t, \tag{20}$$

where $\psi(t)$ is interpolation or shape function and K is number of the recorded temperature samples. Substituting Eq. (20) into Eq. (17) the spatial distribution of the temperature and the thermal flux at some time instant.

$k \cdot \Delta t > t_0$ can be expressed by the next relation:

$$T(x, k\cdot\Delta t) \approx \sum_{j=0}^{k} T_{in}((k-j)\cdot\Delta t)\cdot X_T(x, j) + T_{out}((k-j)\cdot\Delta t)\cdot Y_T(x, j)$$
$$q(x, k\cdot\Delta t) \approx \sum_{j=0}^{k} T_{in}((k-j)\cdot\Delta t)\cdot X_q(x, j) + T_{out}((k-j)\cdot\Delta t)\cdot Y_q(x, j) \quad (21)$$

where the pairs (X_T, Y_T) and (X_q, Y_q) are TRF for temperature and thermal flux respectively. TRF (X_T, Y_T) and (X_q, Y_q) are given by the following relations:

$$X_T(x, j) = g_1 * \psi = \int_{-\Delta t_1}^{\Delta t_2} g_1(x, j\cdot\Delta t - s)\cdot\psi(s)\cdot ds$$
$$Y_T(x, j) = g_2 * \psi = \int_{-\Delta t_1}^{\Delta t_2} g_2(x, j\cdot\Delta t - s)\cdot\psi(s)\cdot ds$$
$$X_q(x, j) = -\lambda_n\cdot\frac{\partial X_T(x,j)}{\partial x} = -\lambda_n\cdot\int_{-\Delta t_1}^{\Delta t_2}\frac{\partial g_1(x, j\cdot\Delta t - s)}{\partial x}\cdot\psi(s)\cdot ds$$
$$Y_q(x, j) = -\lambda_n\cdot\frac{\partial Y_T(x,j)}{\partial x} = -\lambda_n\cdot\int_{-\Delta t_1}^{\Delta t_2}\frac{\partial g_2(x, j\cdot\Delta t - s)}{\partial x}\cdot\psi(s)\cdot ds$$
$$x \in [x_{n-1}, x_n];\ 0 \le j \le k;\ \ \Delta t_1 = \Delta t,\ j < k;\ \ \Delta t_1 = 0,\ j = k;\ \ \Delta t_2 = \Delta t,\ j > 0;\ \ \Delta t_2 = 0,\ j = 0. \quad (22)$$

On this way the pairs of TRF relate temperature and thermal flux inside the wall with recorded surface temperatures at discrete time instants. For $j > k$ TRF are identically equal to zero. The detailed mathematical derivations related to Eqs. (21, 22) are provide in Appendix B.

For simplicity it has been assumed that shape function have non zero values on interval $[-\Delta t, \Delta t]$. To take into account the whole temperature history of the considered structure the series in Eq. (21) should be infinite. This will correspond to the case when the initial conditions in Eq. (1) are taken at minus infinity. As we assume that influence of initial conditions can be neglected after some time t_0 the series in Eq. (21) is truncated and ended at $j = k$. In the general case the developed approach allows the use of the arbitrary shape function $\psi(t)$ in TRF calculation. The train of unit triangle pulses have been widely used in TRF and CTF calculations as shape function [29–31]. According to the procedure presented Appendix A the following analytical relations for TRF are obtained:

$$X_T(x, j=0) = \Delta_1(x) + \lambda_1\cdot\sum_{i=1}^{M}\varphi_i(x)\cdot w_{i,3}\cdot\frac{\partial\varphi_i}{\partial x}\Big|_{x=0}$$
$$X_T(x, j) = \lambda_1\cdot\sum_{i=1}^{M}\exp(-2\cdot m_j\cdot\beta_i^2\cdot\Delta t)\cdot\varphi_i(x)\cdot w_{i,2}\cdot\frac{\partial\varphi_i}{\partial x}\Big|_{x=0},\ j - odd,$$
$$X_T(x, j) = \lambda_1\cdot\sum_{i=1}^{M}(\exp(-2\cdot m_j\cdot\beta_i^2\cdot\Delta t)\cdot w_{i,1} + \exp(-2\cdot(m_j+1)\cdot\beta_i^2\cdot\Delta t)\cdot w_{i,3})\cdot\varphi_i(x)\cdot\frac{\partial\varphi_i}{\partial x}\Big|_{x=0},\ j - even,$$
$$m_j = \frac{j+1-mod_2(j+1)}{2} - 1, \quad (23)$$

where analogue relations for $Y_T(x, j)$ holds. The TRF $X_q(x, j)$ and $Y_q(x, j)$ can be obtained from general relations in Eq. (22).

The above relations are evaluated for the specific case when the shape functions are Lagrange interpolation polynomials of the 2nd order. On the other hand Eq. (22) has general character and can be used for the TRF calculation with any type of the shape functions also according above analysis the next relations are follow:

$X_T(x = 0, j) = \delta_{j0}$ and $Y_T(x = L, j) = \delta_{j0}$ and $X_q(x = L, j) = Y_q(x = 0, j)$.

4. Results and discussion

To validate developed approach the in-situ measurements has been performed and the inside and outside surface temperatures and outside thermal flux has been recorded in period of 360 h with sampling time equal to 5 min in the real environmental conditions.

To filter out the influence of the noise from the measured (raw) data the LOESS smoothing method has been utilized. The recorded and smoothed temperature data are presented in Fig. 3. The periodic variations in the outside surface temperature correspond to daily

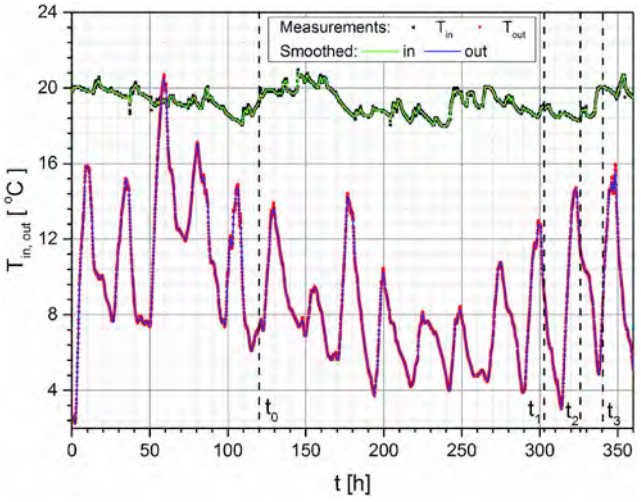

Fig. 3. The inside and outside surface temperature recorded during in-situ measurements in the time period of 360 h with sampling time equal to 5 min.

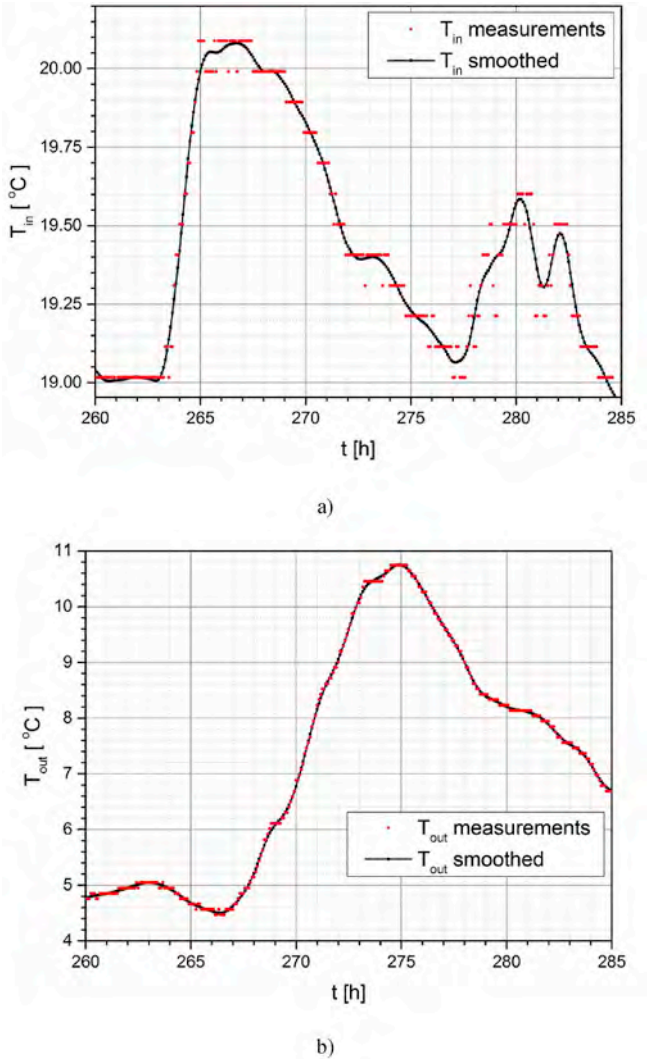

Fig. 4. The comparison between measured (raw) and smoothed surface temperature data from 260 h to 285 h. a) inside, b) outside.

Table 2
First nine eigenvalues for the considered heat conduction problem under Dirichelt BC.

	1	2	3	4	5	6	7	8	9
β_i	0.003898	0.0113	0.01883	0.02642	0.03348	0.03492	0.041989	0.04685	0.04978

variations of the environmental conditions, while the variations of the inside temperature are much smaller. According to analysis in section 2, to exclude influence of unknown initial conditions all results are evaluated for $>t_0$, where $t_o = 120\,h$.

The spatial distribution of the temperature and the heat flux are obtained at time instants $t_{1\text{-}3}$ at the end of this section. The closer and more detailed comparison between smoothed and measured data, for time period 260–285 h, for inside and outside surface temperatures are presented in Fig. 4a and b respectively.

The composite five-layer building wall with dimensions and thermal parameters from Table 1 has been considered as planar structure and conductive heat transfer with Dirichlet BC is modeled by the one-dimensional heat equation given by Eq. (1). This approximation is valid if the lateral dimensions of the wall are much larger than its thickness and if the considered region is far from the wall's edges so that influence of 2D and 3D thermal bridges on the considered thermal flux distribution can be neglected. This condition is satisfied in the most practical situations for the central part of the planar building walls [33]. The thickness of the whole structure was $L = 0.42\,m$.

The eigenvalue problem defined by Eq. (6) was considered. The 8×8 homogeneous system has been assembled according to Eq. (8). To have non-trivial solution it is required that the determinant of the system is equal to zero. This leads to transcendental equation with infinite number of roots which are eigenvalues β_i of the considered problem in Eq. (6). The numerical values of the first nine eigenvalues for ideal thermal contacts between layers ($r_n = 0$) are shown in Table 2.

Corresponding normalized eigenfunctions φ_i have been obtained using procedure from section 3 while the TRF are calculated using Eq. (23). The obtained results are compared with numerical simulations which have been evaluated by the FVM with 2 mm and 10 s spatial and temporal discretization steps respectively. The first nine eigenfunctions which correspond to eigenvalues from Table 2 are presented in Fig. 5a–c.

In Fig. 5d the eigenfunction φ_3 for four different values of the ITRs is presented. The ITRs are included in the model as the equivalent air gap, which was the same between all layers, and equal to 0, 0.5, 1 and 2 mm. It has been assumed that thermal conductivity for air is equal to 0.025 W/m·K [21,25]. Accordingly equivalent air gap of 0.5, 1 and

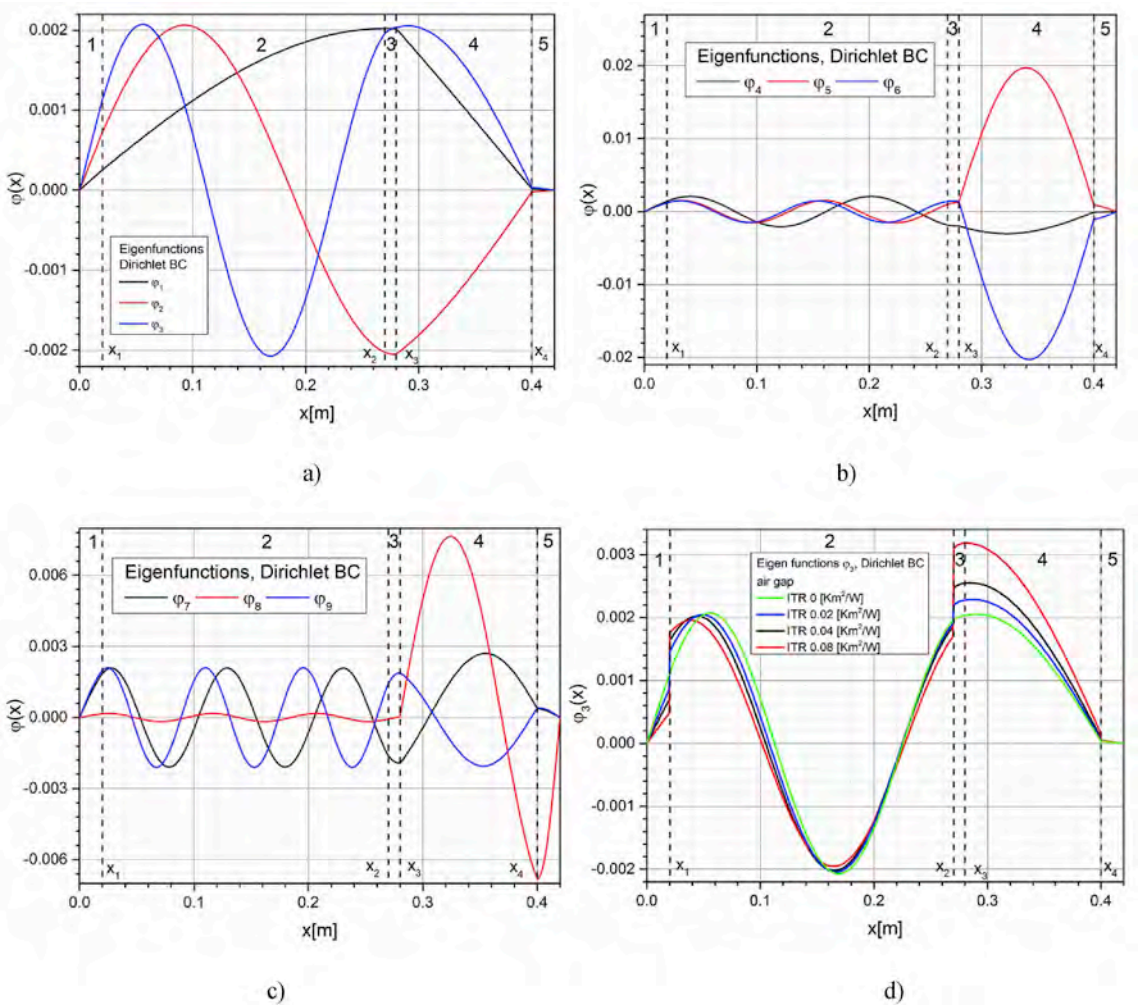

Fig. 5. a–c) The first nine eigenfunctions corresponding to eigenvalues β_i shown in Table 2 with ideal thermal contact between layers. d) The eigenfunction φ_3 for ITR equal to 0, 0.02, 0.04 and 0.08 Km^2/W.

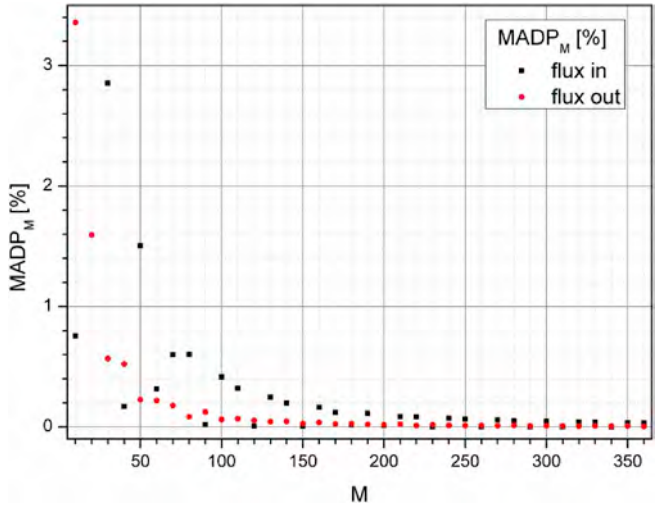

Fig. 6. MADP between two thermal fluxes obtained for two different numbers of terms in truncated TRF sums, M and $M + \Delta M$ ($\Delta M = 10$) for inside and outside surfaces as a function of M.

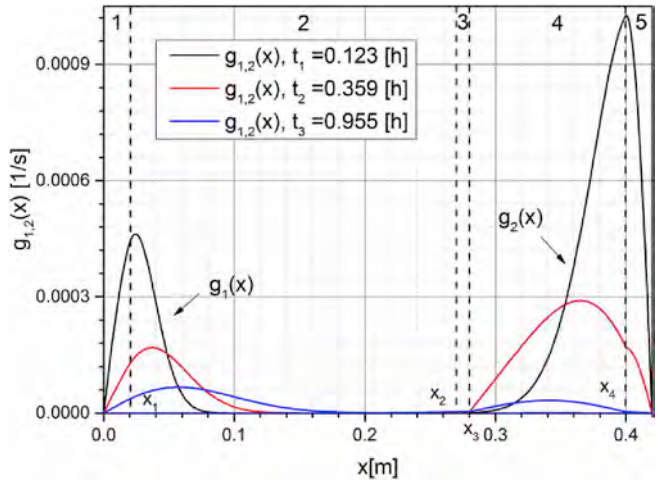

Fig. 7. The spatial distribution of GF $g_{1,2}$ inside considered structure for three different time instants.

2 mm correspond to ITR values equal to: 0.02, 0.04 and 0.08 Km^2/W respectively. The positions of the layer-interfaces are marked with dashed-lines at coordinates $x_{1\text{-}5}$, while the layers are labeled from 1 to 5.

The layer interfaces are marked with dashed lines at coordinates $x_{1\text{-}5}$, while the layers are labeled from 1 to 5.

The convergence analysis is conducted by calculating the thermal fluxes on inside and outside wall surfaces using the measured surface temperatures for different number of terms in truncated infinite series. The relative difference between two thermal fluxes obtained for two different numbers of terms in truncated TRF sums is expressed as Mean Absolute Deviation Percent (MADP) given by the next relation:

$$\mathrm{MADP} = \frac{\sum_{i=1}^{K} |q_i^{M+\Delta M} - q_i^{M}|}{\sum_{i=1}^{K} |q_i^{M}|} \cdot 100[\%] \tag{24}$$

where q_i^M and $q_i^{M+\Delta M}$ are calculated thermal fluxes at ith sampling time obtained for M and $M + \Delta M$ number of terms in truncated TRF sums respectively. The MADP for inside and outside surface fluxes as a function of the number of terms M for $\Delta M = 10$ is shown in Fig. 6.

It can be seen that the MADP in the both cases are less than 0.1% for $M > 200$. Following this analysis the truncated TRF sums with $M = 202$ terms are used in the presented analysis. By further increase of the number of terms obtained results has not been considerably changed.

The spatial distribution of GF $g_{1,2}$ inside considered structure with ideal thermal contact between layers for three different time instants namely: $t_1 = 0.123\,h$, $t_2 = 0.359\,h$ and $t_3 = 0.955\,h$ are presented in Fig. 7.

The layer-interfaces are marked on the same way as in the previous cases. It can be noticed that due to influence of insulation layer g_2 take larger values than g_1, which means that temperature pulse penetrates inside the wall much easier from internal then external side of the structure.

In Fig. 8a and b the temporal distribution of $g_{1,2}$ with ideal thermal contact between layers at three different spatial coordinates are presented, the time instants at which the maximal values are reached are shown as well. These functions represent the response to temperature excitation by Dirac delta temperature pulse from internal and external side of the wall respectively. These results show how temperature response penetrates inside the wall structure during the time from internal.

(g_1) and external side (g_2). From the presented results can be seen that temperature response from internal side penetrates through the first three layers to the point with coordinate 0.37 m in the insulation layer during the time period of approximately 8.24 h which corresponds to maximum of the blue curve in Fig. 8a. After this period the temperature response exponentially vanishes. Fig. 8b shows that the temperature response from external side of the wall penetrates to the same point (0.37 m) for approximately 0.141 h which corresponds to maximum of red curve on the same figure. After this period the g_2 rapidly decrease due to presence of the insulation layer. The presented analysis

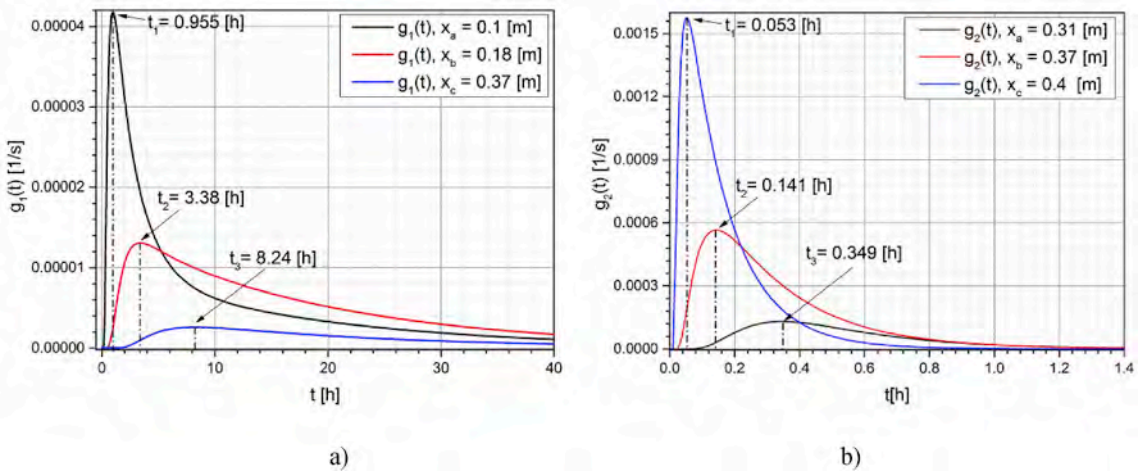

Fig. 8. The temporal distribution of $g_{1,2}$ for three different spatial coordinates.

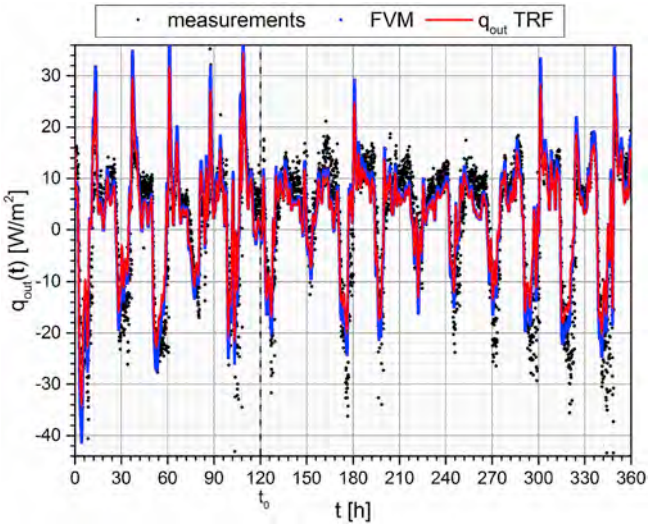

Fig. 9. The Comparison between surface heat flux from the external side of building wall obtained by the measurements, TRF calculations and FVM simulation.

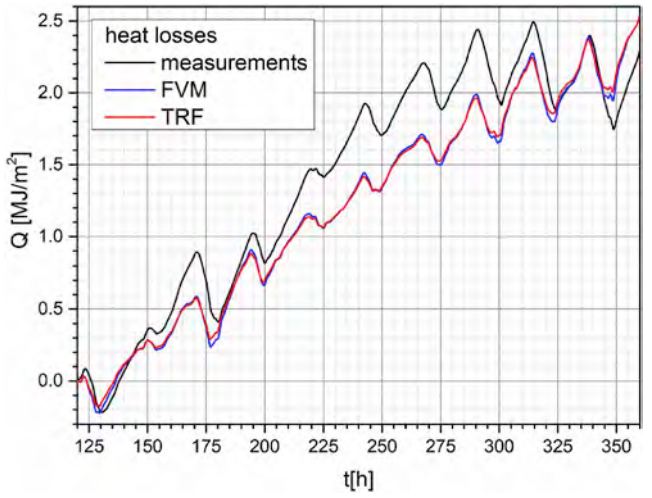

Fig. 10. The heat losses through external side of the wall obtained from flux measurements, TRF calculations and FVM simulation.

demonstrates that arrangement of composite layers and their physical performances has huge influence on the asymptotic behaviour of GF. Accordingly, the rate of change of g_1 in asymptotic region after extremum is much smaller than corresponding rate of change of g_2. This effect is result of the influence of higher thermal capacity of internal layers then insulation one. Because of this the temporal distribution of function g_1 has longer "tail" than g_2. This is in agreement with results presented in Fig. 7.

The comparison between surface heat flux from the external side of building wall ($x = L$) obtained by the measurements, TRF calculations with ideal thermal contact between layers and FVM simulation is presented in Fig. 9. As the measured and calculated flux is determined relative to the direction of x-axes as reference direction, as it is shown in Fig. 2, the positive values of the heat flux correspond to the heat losses when the heat goes outside the building while the negative flux peaks correspond to daily heat gains. As already mentioned at the beginning of this section to exclude the influence of initial conditions the convolution integral has been evaluated from the initial time $t = 0$ h while the validation is performed during the period 120–360 h.

The Mean Absolut Error (MAE) for calculated outside surface heat flux obtained by the TRF calculations and FVM relative to raw

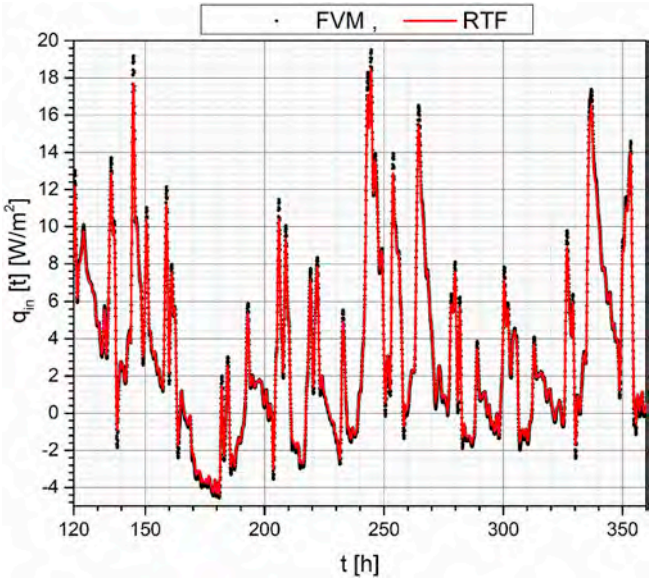

Fig. 11. The surface heat flux from the internal side of building wall obtained by the TRF calculations and FVM simulation.

experimental data are 5.17 W/m^2 and 4.75 W/m^2 respectively, MAE is calculated using the next relation:

$$\mathrm{MAE} = \frac{\sum_{i=1}^{K} |q_i^{calc} - q_i^{raw}|}{K}, \tag{25}$$

where q_i^{calc} and q_i^{raw} are calculated and measured heat surface fluxes from external side of wall at ith sampling time respectively. The MAE between raw experimental data and TRF calculations with equivalent air gap between all layers equal to 0.5, 1 and 2 mm was 5.20, 5.22 and 5.27 W/m^2 respectively. From this analysis follows that deviation from measurement data for considered building structure increases when taking into account the influence of the ITR.

The heat losses through the external side of the wall obtained from the flux measurements, the TRF calculations and FVM is shown in Fig. 10. The heat loss through the external side of the wall Q_{out} is the amount of the heat energy per unit area passing through the external surface during some period of time, and it is defined by the following relation: $Q_{out}(t) = \int_{t_0}^{t} q_{out}(\tau)\cdot d\tau;\ \ t > t_0$.

Mean Absolute Deviation Percent (MADP) error between results obtained from experimental data and TRF calculation and between experimental data and the FVM are: 16.215% and 16.09% respectively, where MADP was calculated using Eq. (24)

The disagreement between measurements data and numerical results can be explained by the influences of the different environmental, constructive and outside factors which have not been included in the present mathematical model such are: indirect sun radiation, three dimensional structures of the building walls, inhomogeneities inside the building materials and uncertainty in the thermal parameters. The possible uncertainty and random influence of the outside environmental factors on thermal parameters could be analyzed using the stochastic approach [24,25].

The MADP error of about 16% is due to cumulative influence of the error in heat flux on the heat losses. The errors in heat flux are especially apparent at positive flux peaks between 150 and 300 h, because of this deviation the heat losses are under-predicted in the same time interval.

The surface heat flux from the internal side of the building wall obtained by the TRF calculations and FVM simulation is presented in Fig. 11.

The Mean Absolut Error (MAE) for inside surface heat flux between

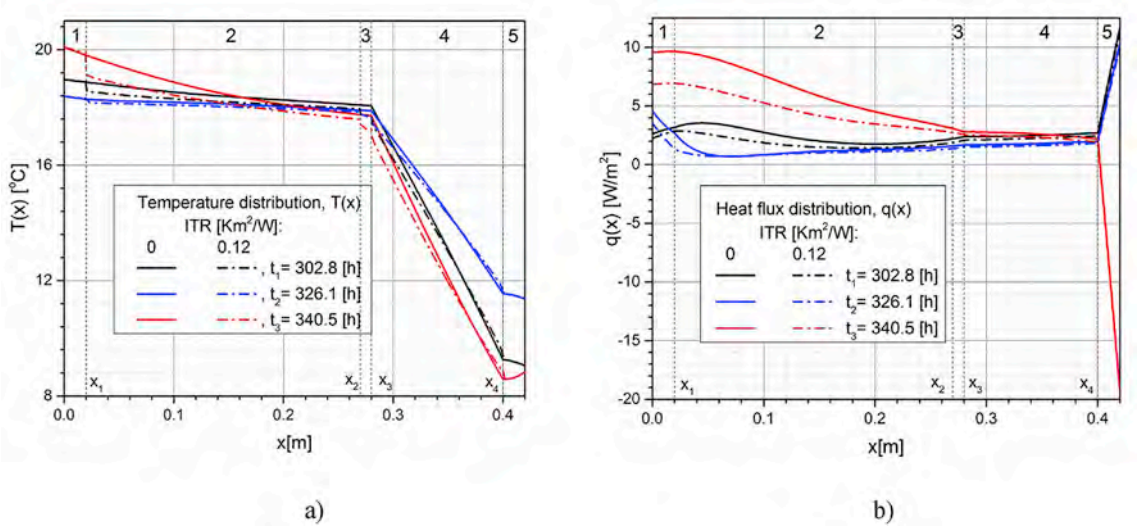

Fig. 12. The spatial distributions of the temperature and the heat flux inside the wall for ITR equal to 0 and 0.12 Km^2/W: a) temperature distribution b) heat flux distribution.

results obtained by the TRF calculations and FVM simulation are 0.348 W/m^2. The largest difference between TRF calculation and FVM simulations are on the inside and outside wall surfaces while there are good agreement inside the wall where the relative difference for spatial and temporal distribution of the temperature and thermal flux was less than 1.0%.

The spatial distribution of the temperature and the heat flux inside considered building wall for ideal thermal contacts between layers and for ITR equal to 0.12 Km^2/W (equivalent air gap 3 mm) at all interfaces at three different time instants $t_1 = 302.8\,h$, $t_2 = 326.1\,h$ and $t_3 = 340.5\,h$ obtained by the TRF calculations are presented in Fig. 12a and b respectively. The time instants $t_{1\text{-}3}$ are denoted with dashed lines in Fig. 3. The heat flux has rapid variations inside the external layer, especially on its external surface, where it changes the sign due to daily variations in external temperature. On the other side the flux variations in the insulation layer, between points x_3 and x_4 is much smaller due to small value of the thermal conductivity in this layer. From the presented results follows that influence of the ITR on the heat flux distribution is much higher near to the inside than outside wall surface. This is due to fact that heat losses on the outside surface are dominantly determined by the presence of the insulation layer, on this way the ITR influence on the heat flux near to the outside wall surface are suppressed and masked by the thermal insulation layer. Nevertheless, for non-ideal thermal contact between layers, there is temperature jump on the interface which is proportional to the heat flux and ITR.

The temporal distribution of the temperatures and the heat flux at three characteristic points $x_1 = 0.02$ m, $x_3 = 0.28$ m and $x_4 = 0.4$ m during the time period of 240 h obtained by the TRF calculations are shown in Fig. 13a and b respectively. The points $x_{1,3,4}$ correspond to interfaces between different layers inside the considered structure and they are marked with dotted lines in Fig. 12a. The influence of the ITR is illustrated by temporal distribution of the temperature and heat flux at spatial coordinate x_4 for two values of ITR, equal to 0 and 0.12 Km^2/W (equivalent air gap: 0 and 3 mm). From Fig. 13a and b follows that this influence is reflected in decrease of magnitude of the heat flux variations, on the other hand the temperature variations are shifted to the higher values, while its magnitude is maintained at the same level.

It could be noticed that the temperature variations in the internal region of the wall, near to x_1 and x_3 are much smaller than in the insulation region near to x_4. On the other side the contrary conclusion can be drawn for the variations of thermal flux, which is smaller in the insulation layer then in the other layers which is in agreement with

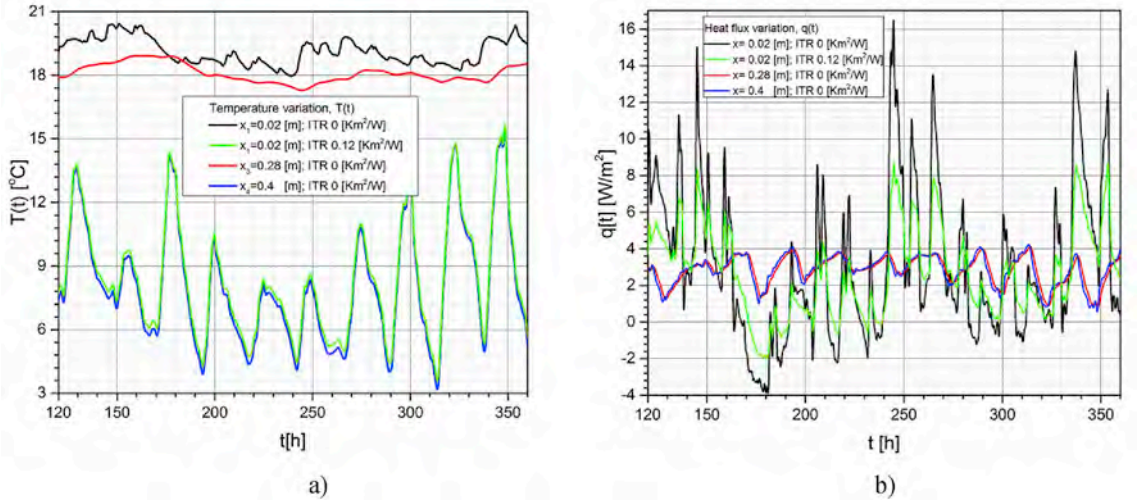

Fig. 13. Temporal distributions of the temperatures and the heat flux at three different points, $x_1 = 0.02$ m, $x_3 = 0.28$ m and $x_4 = 0.4$ m for ITR equal to 0 and 0.12 Km^2/W: a) temperature b) thermal flux.

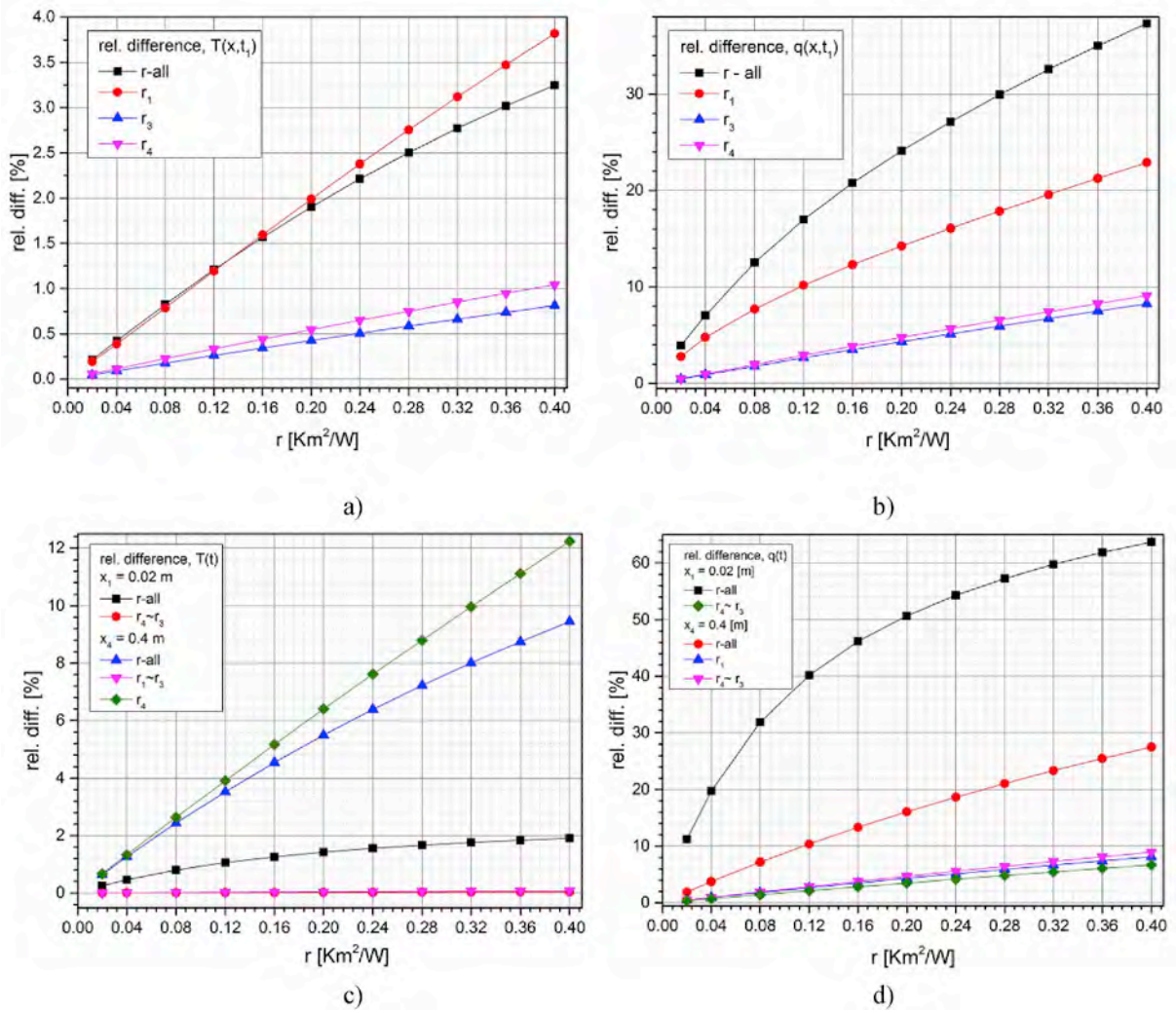

Fig. 14. The MADP [%] difference between spatial (at $t_1 = 302.8\,h$) and temporal (at x_1 and x_4) temperature and thermal flux distributions for the considered wall with ideal thermal contacts and the same wall with different configurations of the ITR: a) spatial temperature distributions b) spatial thermal flux distributions. c) temporal temperature distributions d) temporal flux distributions.

results presented in Fig. 12b.

The relative MADP [%] differences between spatial temperature and heat flux distributions at $t_1 = 302.8$ [h] for considered building wall with the ideal thermal contact and for the same wall with different configurations of the ITR has been shown in Fig. 14a and b respectively. The ITR configurations are denoted as follows: "r-all" – the same thermal resistance is present on the all layer contacts, "r_1", "r_3" and "r_4" the thermal resistances are present only on the one interface at once, namely first, third or fourth interface respectively, where the interfaces are numerated according to Fig. 1 and previous analysis. For the spatial distributions the 840 equidistant spatial samples has been used in Eq. (24) for MADP calculation. It could be seen that the greatest influence on temperature and heat flux distribution have configurations "r-all" and "r_1" which means that the ITR at the first interface has the greatest individual influence on the spatial temperature and heat flux distribution. The relative MADP [%] differences between temporal temperature and heat flux distributions at x_1 and x_4 for the considered building wall with the ideal thermal contact and for the same wall with different configurations of the ITR has been shown in Figs. 14c and d respectively.

The configurations "r_4" and "r_3" for temporal temperature and thermal flux variations at x_1 have almost the same relative differences. The same goes for the configurations "r_1" and "r_3" for temperature variations and for the configurations "r_4" and "r_3" for thermal flux variations at x_2. These relations are denoted with "~" in the figure's legend. From the results presented in Fig. 14c follows that the greatest influence on temperature variations at x_1 has configurations "r-all" while configurations "r-all" and "r_4" have the greatest influence on the temperature variations at x_2. The influence of the other configurations on the temperature variations is negligible. On the similar manner from the results in Fig. 14d follows that the configuration "r-all" has the greatest influence on the thermal flux variations near to internal surface. In the all presented cases in Fig. 14 a-d the MADP differences are presented as function of the ITR in the range from 0.02 to 0.4 Km^2/W (0.5–10 mm in terms of the equivalent air gap).

5. Conclusion

The conductive heat transfer in composite planar structure has been considered. The analytical solution based on GF in time domain for arbitrary number of layers is evaluated in the general case which can be implemented with different type of BC. The novel approach for calculation of TRF based on GF has been proposed. It has been shown that TRF for spatial and temporal distribution of the temperature and the heat flux can be evaluated from GF with arbitrary shape functions. The proposed approach has advantage in comparison with analysis in frequency domain as corresponding eigenvalue problem is solved only once and obtained GF can be reused in calculations of the temperature

and thermal flux at different spatial points. Nevertheless, as the whole analysis is performed in the time domain, it avoids searching poles in the complex plane. The presented numerical procedure employs a truncated series expansion which inevitably produces numerical error. According to conducted analysis the convergence are achieved, with MADP between calculate thermal fluxes less than 0.1%, after 200 TRF terms. It has been shown that arrangement of composite layers and their thermal properties has huge influence on spatial and temporal distribution of GF and behaviour of building structure in dynamical conditions. The largest variations in dynamical regime occur at the outer surfaces while there are slight changes inside insulation layer.

The developed method was validated using in-situ measurements on the five-layer building wall. The internal and external surface temperature and external heat flux have been recorded during the time period of 360 h in real environmental conditions. To exclude influence of unknown initial conditions only results obtained using GF after initial 120 h are compared with experimental data.

The temperature measurements are used as input set of data, while the outside surface heat flux and heat losses obtained by the TRF calculations and FVM have been compared with experimental results. The MAE for external surface heat flux for ideal thermal contacts between layers obtained by TRF and FVM relative to measured data were 5.17 W/m^2 and 4.75 W/m^2 respectively while the MAE between the TRF calculation and FVM for inside surface heat flux was 0.348 W/m^2. The MAE for external surface heat flux has been increased taking into account the influence of the ITR.

The corresponding MADP errors for heat losses obtained using the TRF and FVM relative to measured data were: 16.215% and 16.09% respectively. The largest differences between results obtained by the TRF and FVM was on the inside and outside wall surfaces while there was good agreement inside the wall.

Founding sources

This research did not receive any specific grant from funding agencies in the public, commercial, or not-for-profit sectors.

Appendix A

In practical application the surface temperatures T_{in} and T_{out} in Eqs. (17) and (19) are recorded at discrete time points with some sampling frequency and convolution integral must be evaluated numerically. If the temperatures are recorded at equidistant sampling time intervals Δt the convolution integral from Eq. (17) at some actual time instance $t = k{\cdot}\Delta t$ can be expressed by the next general recursive relation:

$$C_{i,k} = \exp(-\beta_i^2{\cdot}k{\cdot}\Delta t){\cdot}\int_0^{k\cdot\Delta t}\exp(\beta_i^2{\cdot}s){\cdot}D_i(s){\cdot}ds = \exp(-p{\cdot}\beta_i^2{\cdot}\Delta t){\cdot}C_{i,k-p} + \exp(-\beta_i^2{\cdot}k{\cdot}\Delta t){\cdot}\int_{(k-p)\cdot\Delta t}^{k\cdot\Delta t}\exp(\beta_i^2{\cdot}s){\cdot}D_i(s){\cdot}ds, \tag{A1}$$

where p is positive integer, $k > p$ and $D_i(s)$ are functions defined on the following way:

$D_i(s) = \lambda_1{\cdot}T_{in}(s){\cdot}\frac{\partial\varphi_i(x)}{\partial x}\big|_{x=0} - \lambda_N{\cdot}T_{out}(s){\cdot}\frac{\partial\varphi_i(x)}{\partial x}\big|_{x=L}$. The above recursive relation is especially convenient for numerical integration based on Newton-Cotes quadrature. In real measurements the exponential terms in the above integral for large values of β_i is considerably changed during sampling time interval Δt. From this follows that direct numerical evaluation of the last integral with integration step size equal to Δt would produce considerable numerical error in the final results. To avoid this effect and to improve accuracy function $D_i(s)$ can be approximated using Lagrange interpolation polynomials of the 2nd order and recorded data from the three consecutive sampling times: $(k-2){\cdot}\Delta t, (k-1){\cdot}\Delta t, k{\cdot}\Delta t$ on the following way:

$$D_i(s) = \frac{(h-1){\cdot}(h-2)}{2}{\cdot}D_i((k-2){\cdot}\Delta t) - h{\cdot}(h-2){\cdot}D_i((k-1){\cdot}\Delta t) + \frac{(h-1){\cdot}h}{2}{\cdot}D_i(k{\cdot}\Delta t);\ 0 \le h \le 2;\ s = (h+k-2){\cdot}\Delta t \tag{A2}$$

Using above relation the integral in Eq. (A1) can be numerically evaluated by modified Simpson's integration rules which means that $p = 2$ in Eq. (A1) and the next approximate recursive relation is obtained:

$$\exp(-\beta_i^2{\cdot}k{\cdot}\Delta t){\cdot}\int_{(k-2)\cdot\Delta t}^{k\cdot\Delta t}\exp(\beta_i^2{\cdot}s){\cdot}D_i(s){\cdot}ds \approx \sum_{l=1}^{3} w_{i,l}{\cdot}D_i(h_{k,l}{\cdot}\Delta t);\ \ h_{k,l} = (k+l-3){\cdot}\Delta t \tag{A3}$$

where the weights $w_{l=1,2,3}$ are given by the next relations:

$$w_{i,1} = \frac{2-\beta_i^2\cdot\Delta t - \exp(-2\cdot\beta_i^2\cdot\Delta t)\cdot(2+\beta_i^2\cdot\Delta t\cdot(3+2\cdot\beta_i^2\cdot\Delta t))}{2\cdot\Delta t^2\cdot\beta_i^6}$$

$$w_{i,2} = 2{\cdot}\frac{\beta_i^2\cdot\Delta t + \exp(-2\cdot\beta_i^2\cdot\Delta t)\cdot(1+\beta_i^2\cdot\Delta t) - 1}{\Delta t^2\Delta\beta_i^6}$$

$$w_{i,3} = \frac{2+\beta_i^2\cdot\Delta t\cdot(2\cdot\beta_i^2\cdot\Delta t-3) - \exp(-2\cdot\beta_i^2\cdot\Delta t)\cdot(2+\beta_i^2\cdot\Delta t)}{2\cdot\Delta t^2\cdot\beta_i^6} \tag{A4}$$

Utilizing relations in Eq. (A3, A4) in Eq. (A3) the next approximate recursive relation is obtained:

$$C_{i,k} \approx \exp(-2{\cdot}\beta_i^2{\cdot}\Delta t){\cdot}C_{i,k-2} + \sum_{l=1}^{3} w_{i,l}{\cdot}D_i(h_{k,l}{\cdot}\Delta t),\ \ h_{k,l} = (k+l-3) \tag{A5}$$

The numerical evaluation of convolution integrals would be further improved on similar way by using Newton-Cotes quadrature with more interpolation points ($k > 2$).

Appendix B

Using the internal and external interpolated surface temperatures $\tilde{T}_{in,out}(t)$ from Eq. (20) the temperature distribution from Eq. (17) can be expressed such as:

$$T(x,t) = g_1 * \tilde{T}_{in} + g_2 * \tilde{T}_{out} = \Delta_1{\cdot}\tilde{T}_{in}(t) + \Delta_2{\cdot}\tilde{T}_{out}(t) +$$

$$\sum_{i=1}^{M}\varphi_i(x)\cdot\sum_{j_1}^{K}\left[\lambda_1\cdot\frac{\partial\varphi_i}{\partial x}\bigg|_{x=0}\cdot T_{in}(j_1\cdot\Delta t)-\lambda_N\cdot\frac{\partial\varphi_i}{\partial x}\bigg|_{x=L}\cdot T_{out}(j_1\cdot\Delta t)\right]\cdot\int_0^t\exp(-\beta_i^2\cdot(t-s_1))\cdot\psi(s_1-j_1\cdot\Delta t)\cdot ds_1,$$

where $\psi(t)$ is shape function having non-zero values on interval $[-\Delta t, \Delta t]$ and satisfy the following relation:

$\psi(j\cdot\Delta t)=\delta_{j0}$. If the integral in the above relation is evaluated at time instant $t=k\cdot\Delta t>t_0$ and transformed by the change of variables $s=s_1-j_1\cdot\Delta t$ the next relation is obtained:

$$\int_0^{k\cdot\Delta t}\exp(-\beta_i^2\cdot(k\cdot\Delta t-s_1))\cdot\psi(s_1-j_1\cdot\Delta t)\cdot ds_1=\int_{-j_1\cdot\Delta t}^{(k-j_1)\cdot\Delta t}\exp(-\beta_i^2\cdot((k-j_1)\cdot\Delta t-s)\cdot\psi(s)\cdot ds=$$

$$\int_{\Delta t_1}^{\Delta t_2}\exp(-\beta_i^2\cdot((k-j_1)\cdot\Delta t-s)\cdot\psi(s)\cdot ds\ ;$$

$$\Delta t_1=0,\ j_1=0;\quad \Delta t_1=\Delta t,\ 0<j_1\le k;\quad \Delta t_2=0,\ j_1=k;\quad \Delta t_2=\Delta t,\ 0\le j_1<k\ .$$

The above integral has non-zero value only for $0\le j_1\le k$. After these transformations the relation in Eq. (B1) can be expressed in the following compact form:

$$T(x,t)=\sum_{j=0}^{k}T_{in}\cdot((k-1)\cdot\Delta t)\cdot X_T(x,j)+T_{out}\cdot((k-1)\cdot\Delta t)\cdot Y_T(x,j)\ , \tag{B3}$$

where the next change of indices are used: $j=k-j_1,\ 0\le j\le k$ while the functions: $X_T(x,j)$ and $Y_T(x,j)$ are the pair of TRF given such as:

$$X_T(x,j)=\Delta_1(x)\cdot\delta_{j0}+\lambda_1\cdot\sum_{i=1}^{M}I_{i,j}\cdot\varphi_i(x)\cdot\frac{\partial\varphi_i}{\partial x}\Big|_{x=0}$$

$$Y(x,j)=\Delta_2(x)\cdot\delta_{j0}-\lambda_N\cdot\sum_{i=1}^{M}I_{i,j}\cdot\varphi_i(x)\cdot\frac{\partial\varphi_i}{\partial x}\Big|_{x=L}$$

$$I_{i,j}=\int_{\Delta t_1}^{\Delta t_2}\exp(-\beta_i^2\cdot((j\cdot\Delta t-s))\cdot\psi(s)\cdot ds,$$

$$\Delta t_1=0,\ j=k;\quad \Delta t_1=\Delta t,\ 0\le j\le k;\quad \Delta t_2=0,\ j=0;\quad \Delta t_2=\Delta t,\ 0<j<k.$$

References

[1] K. Arendt, M. Krzaczek, Co-simulation strategy of transient CFD and heat transfer in building thermal envelope based on calibrated heat transfer coefficients, Int. J. Therm. Sci. 85 (2014) 1–11 https://doi.org/10.1016/j.ijthermalsci.2014.06.011.

[2] G. Oliveti, N. Arcuri, D. Mazzeo, M. De Simone, A new parameter for the dynamic analysis of building walls using the harmonic method, Int. J. Therm. Sci. 88 (2015) 96–109 https://doi.org/10.1016/j.ijthermalsci.2014.09.006.

[3] Qiuyuan Zhu, Xinhua Xu, Jiajia Gao, Xiao Fu, A semi-dynamic model of active pipe-embedded building envelope for thermal performance evaluation, Int. J. Therm. Sci. 88 (2015) 170–179 https://doi.org/10.1016/j.ijthermalsci.2014.09.014.

[4] Yuming Liu, Tingting Liu, Sudong Ye, Yisheng Liu, Cost-benefit analysis for Energy Efficiency Retrofit of existing buildings: a case study in China, J. Clean. Prod. 177 (2018) 493–506 https://doi.org/10.1016/j.jclepro.2017.12.225.

[5] Yang Wang, Ashish Shukla, Shuli Liu, A state of art review on methodologies for heat transfer and energy flow characteristics of the active building envelopes, Renew. Sustain. Energy Rev. 78 (2017) 1102–1116 https://doi.org/10.1016/j.rser.2017.05.015.

[6] Olatz Pombo, Beatriz Rivela, Javier Neila, The challenge of sustainable building renovation: assessment of current criteria and future outlook, J. Clean. Prod. 123 (2016) 88–100 https://doi.org/10.1016/j.jclepro.2015.06.137.

[7] Haibo Zhang, Wenzhong Wang, Shengguang Zhang, Ziqiang Zhao, Semi-analytic solution of three-dimensional temperature distribution in multilayered materials based on explicit frequency response functions, Int. J. Heat Mass Tran. 118 (2018) 208–222 https://doi.org/10.1016/j.ijheatmasstransfer.2017.10.118.

[8] Jia-meng Tian, Bin Chen, Zhi-fu Zhou, Methodology of surface heat flux estimation for 2D multi-layer mediums, Int. J. Heat Mass Tran. 114 (2017) 675–687 https://doi.org/10.1016/j.ijheatmasstransfer.2017.06.053.

[9] C. Serra, A. Tadeu, N. Simões, Heat transfer modeling using analytical solutions for infrared thermography applications in multilayered buildings systems, Int. J. Heat Mass Tran. 115 (2017) 471–478 https://doi.org/10.1016/j.ijheatmasstransfer.2017.08.042.

[10] Jose Manuel Pinazo Ojer, Victor Manuel Soto Frances, Emilio Sarabia Escriva, Laura Soto Frances, Thermal response factors to a 2nd order shaping function for the calculation of the 1D heat conduction in a multi-layered slab, Int. J. Heat Mass Tran. 88 (2015) 579–590, https://doi.org/10.1016/j.ijheatmasstransfer.2015.04.110.

[11] K.L. Johnson, Contact Mechanics, Cambridge University Press, London, 1987.

[12] Selçuk Erol, François Bertrand, Multilayer analytical model for vertical ground heat exchanger with groundwater flow, Geothermics 71 (2018) 294–305 https://doi.org/10.1016/j.geothermics.2017.09.008.

[13] Hengliang Zhang, Weimin Kan, Xuejiao Hu, Green's function approach to the nonlinear transient heat transfer analysis of functionally graded materials, Int. J. Therm. Sci. 71 (2013) 292–301 https://doi.org/10.1016/j.ijthermalsci.2013.04.025.

[14] B. Babak Dehghan, Ergin Kukrer, A new 1D analytical model for investigating the long term heat transfer rate of a borehole ground heat exchanger by Green's function method, Renew. Energy 108 (2017) 615–621 https://doi.org/10.1016/j.renene.2016.11.002.

[15] Kevin D. Cole, James V. Beck, A. Haji-Sheikh, Bahman Litkouhi, Heat Conduction Using Green's Functions, second ed., A Series of Reference Books and Textbooks, Taylor and Francis Group, New York, 2011.

[16] Zahedeh Bashardanesh, Per Lötstedt, Efficient Green's Function Reaction Dynamics (GFRD) simulations for diffusion-limited, reversible reactions, J. Comput. Phys. 357 (2018) 78–99 https://doi.org/10.1016/j.jcp.2017.12.025.

[17] N. Simões, I. Simões, A. Tadeu, C.A.B. Vasconcellos, W.J. Mansur, 3D transient heat conduction in multilayer systems e Experimental validation of semi-analytical solution, Int. J. Therm. Sci. 57 (2012) 192–203, https://doi.org/10.1016/j.ijthermalsci.2012.02.007.

[18] O.K. Dudko, A.M. Berezhkovskii, G.H. Weiss, Diffusion in the presence of periodically spaced permeable membranes, J. Chem. Phys. 121 (22) (2004) 11283–11288.

[19] Radovan Gospavic, Milesa Sreckovic, Viktor Popov, Goran Todorovic, 3D modeling of material heating with the laser beam for cylindrical geometry, Math. Comput. Model. 43 (2006) 620–631.

[20] N. Simoes, A. Tadeu, Fundamental solutions for transient heat transfer by conduction and convection in an unbounded, half-space, slab and layered media in the frequency domain, Eng. Anal. Bound. Elem. 29 (12) (2005) 1130–1142, https://doi.org/10.1016/j.enganabound.2005.06.002.

[21] H.S. Carslaw, J.C. Jaeger, Conduction of Heat in Solids, second ed., Oxford University Press, London, 1959.

[22] Xiaobing Luo, Zhangming Mao, Sheng Liu, Analytical thermal resistances model for eccentric heat source on rectangular plate with convective cooling at upper and lower surfaces, Int. J. Therm. Sci. 50 (2011) 2198–2204, https://doi.org/10.1016/j.ijthermalsci.2011.06.011.

[23] Dongbin Xiu, George Em Karniadakis, A new stochastic approach to transient heat conduction modeling with uncertainty, Int. J. Heat Mass Tran. 46 (2003) 4681–4693, https://doi.org/10.1016/S0017-9310(03)00299-0.

[24] Dongbin Xiu, Jan S. Hesthaven, High-order collocation methods for differential equations with random inputs, SIAM J. Sci. Comput., Vol. 27, No. 3, pp. 1118–1139, DOI. 10.1137/040615201.

[25] M.N. Ozisik, Heat Conduction, second ed., John Wiley & Sons, United States, 1993.

[26] G.P. Mulholland, M.H. Cobble, Diffusion through composite media, Int. J. Heat Mass Tran. 15 (1) (1972) 147–160 https://doi.org/10.1016/0017-9310(72)90172-X.

[27] A. David, Kopriva, Implementing Spectral Methods for Partial Differential Equations, Springer, 2009, https://doi.org/10.1007/978-90-481-2261-5.

[28] D.G. Stephenson, G.P. Mitalas, Calculation of heat conduction transfer functions for multi-layer slabs, ASHRAE Transact. 77 (2) (1971) 117–126.

[29] Ismael R. Maestre, Paloma R. Cubillas, Luis Pe´rez-Lombard, Transient heat conduction in multi-layer walls: an efficient strategy for Laplace's method, Energy

Build. 42 (2010) 541–546, https://doi.org/10.1016/j.enbuild.2009.10.023.
[30] C. Luo, B. Moghtaderi, A. Page, Modelling of wall heat transfer using modified conduction transfer function, finite volume and complex Fourier analysis methods, Energy Build. 42 (2010) 605–617, https://doi.org/10.1016/j.enbuild.2009.10.031.
[31] Xiang Qian Li, Youming Chen, J.D. Spitler, D. Fisher, Applicability of calculation methods for conduction transfer function of building constructions, Int. J. Therm. Sci. 48 (2009) 1441–1451, https://doi.org/10.1016/j.ijthermalsci.2008.11.006.
[32] https://shop.greenteg.com/; 23 November 2018.
[33] Hugo S.L. Hens, Building Physics - Heat, Air and Moisture: Fundamentals and Engineering Methods with Examples and Exercises, second ed., Ernst & Sohn, Berlin, 2012.
[34] J.P. Holman, Heat Transfer, tenth ed., Mc Graw Hill, Higher Education, Boston, New York, 2010.
[35] Nicolas Young, An Introduction to Hilbert Space, Cambridge University Press, Cambridge, New York, Melbourne, 1988.
[36] C.A. Brebbia, J.C. Tells, L.C. Worbel, Boundary Element Techniques, Springer, Berlin, Heidelberg, New York, Tokyo, 1984.
[37] Radovan Gospavic, Viktor Popova, Milesa Sreckovic, C.S. Chenc, DRM-MD approach for modeling laser–material interaction with axial symmetry, Eng. Anal. Bound. Elem. 31 (2007) 200–208, https://doi.org/10.1016/j.enganabound.2006.09.006.